BIOMATERIALS

Nanofiber-hydrogel composite–mediated angiogenesis for soft tissue reconstruction

Xiaowei Li[1,2,3]*†, Brian Cho[4]*, Russell Martin[1,2,3], Michelle Seu[4], Chi Zhang[1,2,3], Zhengbing Zhou[1,2,3], Ji Suk Choi[1,2,3], Xuesong Jiang[1,2,3], Long Chen[1,2,3], Gurjot Walia[4], Jerry Yan[5], Megan Callanan[5], Huanhuan Liu[1,2,3], Kevin Colbert[1,2], Justin Morrissette-McAlmon[1,5], Warren Grayson[1,2,5], Sashank Reddy[4]‡, Justin M. Sacks[4]‡, Hai-Quan Mao[1,2,3,5]‡

Soft tissue losses from tumor removal, trauma, aging, and congenital malformation affect millions of people each year. Existing options for soft tissue restoration have several drawbacks: Surgical options such as the use of autologous tissue flaps lead to donor site defects, prosthetic implants are prone to foreign body response leading to fibrosis, and fat grafting and dermal fillers are limited to small-volume defects and only provide transient volume restoration. In addition, large-volume fat grafting and other tissue-engineering attempts are hampered by poor vascular ingrowth. Currently, there are no off-the-shelf materials that can fill the volume lost in soft tissue defects while promoting early angiogenesis. Here, we report a nanofiber-hydrogel composite that addresses these issues. By incorporating interfacial bonding between electrospun poly(ε-caprolactone) fibers and a hyaluronic acid hydrogel network, we generated a composite that mimics the microarchitecture and mechanical properties of soft tissue extracellular matrix. Upon subcutaneous injection in a rat model, this composite permitted infiltration of host macrophages and conditioned them into the pro-regenerative phenotype. By secreting pro-angiogenic cytokines and growth factors, these polarized macrophages enabled gradual remodeling and replacement of the composite with vascularized soft tissue. Such host cell infiltration and angiogenesis were also observed in a rabbit model for repairing a soft tissue defect filled with the composite. This injectable nanofiber-hydrogel composite augments native tissue regenerative responses, thus enabling durable soft tissue restoration outcomes.

INTRODUCTION

Loss of soft tissue including skin, fat, and muscle is a ubiquitous problem in clinical medicine. Patients sustain these losses secondary to tumor excision, traumatic injury, congenital malformation, and natural aging. The absence of these tissues leads to major functional and aesthetic disturbances that are difficult to treat by conventional means. Existing options for soft tissue restoration usually involve surgery with its attendant cost and morbidity. In addition to these general inconveniences, each of the most common surgical options has specific drawbacks. Autologous tissue transfer requires moving soft tissues from another part of the body in lengthy surgical procedures that result in donor site deficits (*1*). Prosthetic implants are prone to foreign body responses, leading to fibrosis and encapsulation (*2*). Fat grafting, which involves transplantation of adipocytes harvested during liposuction, is limited to small volumes and is hampered by poor graft survival (*3*). Numerous materials have been developed to overcome these limitations and enable off-the-shelf solutions for soft tissue restoration (*4*). Natural biodegradable materials such as collagen (*5*) and silk (*6*) have been processed into injectable filler gels and foams to reconstruct both small and larger defects. Hydrogels remain the most popular scaffold matrices to support tissue regeneration because of their three-dimensional (3D) nature and elastic properties, which are similar to those of soft tissues (*7*, *8*). Various methods have been used to generate hydrogel fillers with shear storage moduli (G′) similar to that of native fat tissues (150 to 500 Pa) (*9*), so they may maintain their unique volume and shape against physical stress from the surrounding tissue. To date, these resilient structural properties have been achieved at the expense of high cross-linking density and small average pore size in the hydrogel networks (*10*), leading to limited cellular infiltration and consequently poor regeneration.

Porosity and pore size of the implant materials can influence host biological responses because of their effect on macrophage infiltration and activities (*11*). Several studies have shown that skewed polarization of macrophages triggered by pore features and mechanical property of the scaffold can influence the degree of fibrosis and scar formation (M1 macrophage-dominant response) versus angiogenesis and matrix remodeling (M2 macrophage-dominant response) (*11*, *12*). Porous materials implanted in soft tissues, compared with nonporous implants, modulated pro-regenerative polarization of macrophages, promoted angiogenesis, and reduced fibrosis and scar formation (*13*). Therefore, the ability for hydrogel scaffolds to promote cellular infiltration and vascular ingrowth is key to modulating acute and chronic inflammation, promoting tissue remodeling, angiogenesis, and regeneration, and achieving a long-lasting soft tissue restoration.

Electrospun nanofiber meshes have often been used as tissue-engineering substrates because of their topographical similarity to the native extracellular matrix (ECM). The decellularized ECM of adipose tissue is highly fibrous and porous (*7*, *14*). However, these mesh-like matrices are not injectable and do not provide the defined volume or the mechanical properties necessary for adipose tissue reconstruction.

[1]Translational Tissue Engineering Center, Johns Hopkins School of Medicine, Baltimore, MD 21287, USA. [2]Institute for NanoBioTechnology, Johns Hopkins University, Baltimore, MD 21218, USA. [3]Department of Materials Science and Engineering, Johns Hopkins University, Baltimore, MD 21218, USA. [4]Department of Plastic and Reconstructive Surgery, Johns Hopkins School of Medicine, Baltimore, MD 21287, USA. [5]Department of Biomedical Engineering, Johns Hopkins School of Medicine, Baltimore, MD 21205, USA.
*These authors contributed equally to this work.
†Present address: Mary and Dick Holland Regenerative Medicine Program, Department of Neurological Sciences, University of Nebraska Medical Center, Omaha, NE 68198, USA.
‡Corresponding author. Email: hmao@jhu.edu (H.-Q.M.); jmsacks@jhmi.edu (J.M.S.); sreddy6@jhmi.edu (S.R.)

Adding fibrous components to polyethylene glycol (PEG), polyacrylamide, or alginate hydrogels during gelation moderately improves their mechanical properties for cartilage and bone tissue engineering (*15*, *16*). These reported materials have relatively high shear moduli in the range of 5 to 50 kPa. They are not expected to allow cell infiltration because of their relatively low pore sizes, even when adipocyte adhesive ligands are present. In addition, these hydrogels are typically nondegradable or have very slow degradation rates. None of these reported materials for soft tissue restoration—neither hydrogel networks nor ECM mimetic meshes—have simultaneously met the requirements for structural integrity conferred by sufficient mechanical property, high matrix porosity, and pore size that enables cellular infiltration, vascularization, and tissue remodeling.

To satisfy the competing yet critical requirements for structural integrity and cellular ingrowth (porosity and pore size), we developed a hyaluronic acid (HA) hydrogel composite covalently linked to fragmented electrospun poly(ε-caprolactone) (PCL) nanofibers. Using a thiolated HA (HA-SH)/PEG diacrylate (PEGDA) hydrogel developed previously by Shu *et al*. (*17*), we introduced interfacial bonding between the HA-SH/PEGDA hydrogel network and surface-functionalized PCL nanofibers. This composite design gives the material higher bulk porosity and cell permeability while achieving sufficiently high storage modulus necessary for the composite to match the mechanical properties of natural adipose tissue. Here, we show that this chemically integrated composite structure has improved mechanical properties over a mixture of fibers and hydrogel, particularly for hydrogels with low stiffness, and investigate the effects on macrophage infiltration and polarization and angiogenic response from the surrounding tissue.

RESULTS

Engineering a fiber-hydrogel composite with interfacial bonding

We designed a unique composite scaffold by bonding biodegradable PCL fiber surface with HA hydrogel molecular network. To achieve this, we first introduced carboxyl groups to PCL fiber surface through plasma activation according to our previous report (*18*). The surface carboxylic group density could be varied between 75 and 150 nmol/mg of fibers by adjusting plasma treatment time (fig. S1). A small fraction (1 to 3%) of the carboxyl group was converted to the thiol-reactive maleimide (MAL) group to generate MAL-functionalized PCL (MAL-PCL) fibers. MAL-PCL fibers were then fragmented in a cryogenic milling chamber filled with liquid nitrogen. We controlled the average length of the fibers within the range of 20 to 100 μm by adjusting the duration of the cooling and milling cycles (fig. S2). The MAL-PCL fiber fragments were then mixed with the HA hydrogel precursors at predetermined ratios to form composite. During the gelation process, MAL-PCL fiber fragments were conjugated to HA-SH cross-linked network, forming interfacial covalent bonds and then generating an integrated composite structure (Fig. 1A and fig. S3). Scanning electron microscopy images revealed that these fibers were connected to the dried HA hydrogel network, exhibiting a fibrillar microarchitecture similar to what was observed in native adipose tissue ECM (Fig. 1, B and C). A marked reinforcement effect was observed when these fibers were bonded in the HA hydrogel matrix (Fig. 1D). Furthermore, the composite component premix could readily pass through a 30-gauge needle within 30 min after mixing (Fig. 1E). The passage through the needle did not induce separation of the fibers from the hydrogel phase nor did it affect gelation kinetics (fig. S4). After complete gelation, PCL fiber fragments were distributed relatively evenly throughout the hydrogel (fig. S5). In contrast, unmodified PCL fibers and carboxyl-functionalized PCL fibers blended into the same HA hydrogel without interfacial bonding phase-separated easily (fig. S6).

To quantitatively analyze the interfacial bonding between PCL fiber and HA hydrogel, we examined the G_0' of the HA hydrogel phase and overall G′ of the composite. In an oscillatory strain sweep test with only 1 to 2% (w/w) of fiber loading in the composite, the G′ of a composite with fibers having surface MAL groups was two to fivefold higher than that without interfacial bonding ($P < 0.0001$; Fig. 1, F and G). G′ of the composites increased with the increase of fiber and cross-linker PEGDA concentrations. This allowed us to generate composites with G′ in the range of 150 to 600 Pa, similar to that of native fat tissue, while starting from HA hydrogels with an initial G_0' of 80 to 220 Pa.

Improved cell migration and vascular-like network formation inside composite

To investigate cell migration inside our composite, we seeded human adipose-derived stem cell (hASC) spheroids (uniformly generated with a diameter of ~200 μm) inside the composite and imaged cell spreading as a function of time (*19*). We seeded hASC spheroids within a composite (G′ = 150 Pa and G_0' = 80 Pa) and the corresponding HA hydrogel controls (G′ = 80 and 150 Pa) and cultured them for 14 days. No noticeable cell migration was observed inside the 150-Pa hydrogel (Fig. 2A), consistent with our previous studies that showed stem cells could not migrate inside an HA hydrogel matrix when the G′ of the hydrogel was more than 100 Pa (*19*, *20*). In contrast, hASCs within the 150-Pa composite migrated the longest distance when compared to those in the 80- and 150-Pa hydrogels [composite group: 207 μm, 80-Pa hydrogel group: 145 μm ($P < 0.01$), and 150-Pa hydrogel group: 0 μm ($P < 0.0001$); Fig. 2B]. They migrated effectively in 3D culture and formed networks in the 150-Pa composite (Fig. 2C). In addition, nanofibers were distributed relatively uniformly throughout the hydrogel.

To further evaluate cell migration and organization inside the fiber-hydrogel composite, we used an established in vitro vascularization model (*21*). Single hASCs were cocultured with endothelial cells inside the 80- and 150-Pa hydrogels and the 150-Pa composite. We selected the 80-Pa hydrogel as a control because vascular-like network formation occurred in this HA hydrogel with a narrow range of G′ around 80 Pa (figs. S7 and S8). These cells inside the 80-Pa hydrogel and the 150-Pa composite spontaneously initiated vascular-like morphogenesis and organized to form multicellular tubular structures with branching and visible open lumen space starting as early as day 2 in culture. Such developments were not seen in the 150-Pa hydrogel. Tubular structural development was more pronounced and progressive in the 150-Pa composite than the 80-Pa hydrogel (Fig. 2D). At day 7 in culture, 3D tubular networks reminiscent of capillaries formed inside both the 80-Pa hydrogel and the 150-Pa composite; however, they were more interconnected and developed highest network density in the 150-Pa composite [total length of interconnected branches per area for the composite group: 12.7 mm/mm^2, 80-Pa hydrogel group: 7.0 mm/mm^2 ($P < 0.01$), and 150-Pa hydrogel group: 1.7 mm/mm^2 ($P < 0.0001$); Fig. 2E].

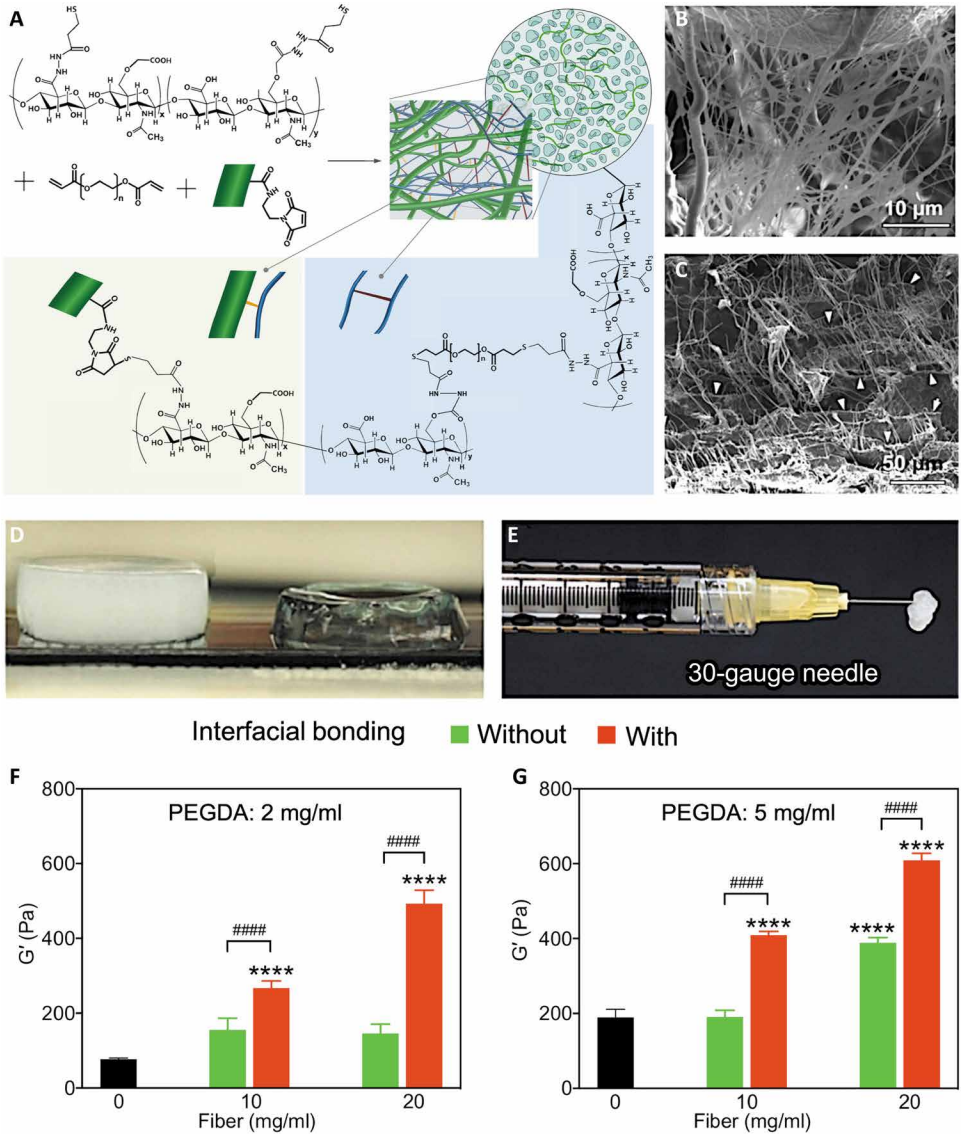

Fig. 1. Engineering a nanofiber-hydrogel composite with interfacial bonding between nanofiber surface and hydrogel network. (**A**) Schematic of the synthesis and structure of PCL nanofiber-HA hydrogel composite. (**B** and **C**) Scanning electron microscopy images of rat native fat tissue (B) and PCL nanofiber-HA hydrogel composite (C) showing that fibers are embedded into the HA hydrogel network (arrowheads). (**D**) Image showing a PCL nanofiber-HA hydrogel composite (G′ = 250 Pa, left) and an HA hydrogel [oscillatory shear storage modulus (G′$_0$) = 80 Pa, right] constructed from the same 80-Pa HA hydrogel. (**E**) Image showing that the composite can be injected through a 30-gauge needle. (**F** and **G**) G′ of HA hydrogels and nanofiber-hydrogel composites with different PEGDA cross-linker concentrations of 2 mg/ml (F) and 5 mg/ml (G) and fiber amounts (0, 10, and 20 mg/ml) with or without interfacial bonding. The concentration of HA was maintained at 4 mg/ml (n = 3 to 9). Statistical significance was calculated by one-way analysis of variance (ANOVA) with the Dunnett's post hoc test. Asterisk (*) indicates the comparison between groups with and without fibers (hydrogel control). Hash key (#) denotes the comparison between groups with and without interfacial bonding. ****P < 0.0001, ####P < 0.0001. Data are presented as means ± SEM.

Enhanced angiogenesis inside composite after subcutaneous implantation in rat model

To investigate composite-mediated host cell infiltration in vivo, we subcutaneously injected the composite (G′ = 150 Pa and G$_0$′ = 80 Pa) and two hydrogel controls (G′ = 80 and 150 Pa) into the backs of Lewis rats. Host vascular endothelial cells (RECA-1$^+$) infiltrated and formed blood vessels inside the 150-Pa composite (figs. S9 to S11). The HA hydrogel with a similar G′ lacked vascular infiltration at postoperative day (POD) 7 (Fig. 3A). The composite group resulted in the highest density of blood vessels among these three groups at POD 7 [composite group: 7.7 mm/mm^2, 80-Pa hydrogel group: 3.5 mm/mm^2 (P < 0.01), and 150-Pa hydrogel group: 1.2 mm/mm^2 (P < 0.001); Fig. 3B and fig. S9]. Concurrent with HA degradation in vivo, vascular cells infiltrated the hydrogels at POD 84; however, they were still fewer and less organized than those in the composite. Well-formed blood vessel networks with a total length of about 19 mm/mm^2 formed inside the composite at POD 84 [composite group: 19.0 mm/mm^2, 80-Pa hydrogel group: 3.3 mm/mm^2 (P < 0.05), and 150-Pa hydrogel group: 3.8 mm/mm^2 (P < 0.05); Fig. 3C and fig. S11]. The blood vessels inside the 150-Pa composite were well developed with continuous endothelial lining and surrounding smooth muscle cells (figs. S12 and S13). These blood vessels were perfusable and functional; this was confirmed by indocyanine green angiography that revealed that host blood could flow into the composite (figs. S14 and S15). Furthermore, the composite exhibited lasting shape retention with gradual host cell infiltration and replacement at POD 84 (Fig. 3A and fig. S11). These results confirm the ability of this composite to facilitate the ingrowth of host blood vessels and highlight the advantage of this composite in satisfying requirements for both mechanical property and porosity.

Infiltration of macrophages and their polarization inside composite

We examined whether improved angiogenesis in the composite correlates with macrophage infiltration and polarization. Activated macrophages exhibit a spectrum of phenotypes. Two classically described groups are the M1 (CD86$^+$) and M2 (CD206$^+$) subtypes, which represent the pro-inflammatory and pro-regenerative phenotypes, respectively (*22*). At POD 7, macrophages rarely infiltrated the 150-Pa hydrogel; however, we identified an ample number of macrophages inside the 150-Pa composite. Among the macrophages found in the composite, a portion of them stained CD206$^+$ and was observed along the fibers at POD 7. These CD206$^+$ macrophages within the composite exhibited an elongated morphology (*23*), which was seldom seen in the hydrogel controls (Fig. 4A). At POD 14, there were still very few macrophages detected in the 150-Pa hydrogel, which was quantitatively validated by flow cytometry (Fig. 4, B to D, and fig. S16). More

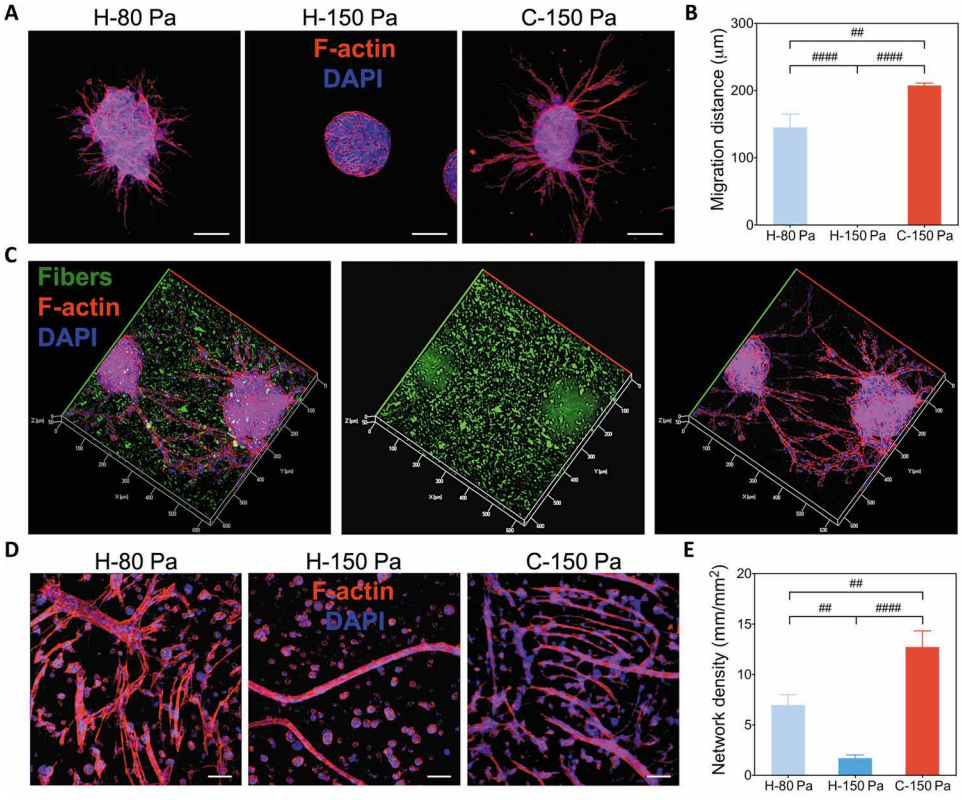

Fig. 2. Enhanced cell migration and vascular-like network formation inside composite. (**A**) hASC migration from 200-μm spheroids embedded in the 80- and 150-Pa HA hydrogels and the 150-Pa composite. (**B**) Quantitative analysis of cell migration distance inside the hydrogels and the composite ($n = 4$ to 7). (**C**) hASCs formed 3D connected networks in the 150-Pa composite. (**D**) Vascular-like network formation in the 80- and 150-Pa hydrogels and the 150-Pa composite. (**E**) Quantitative analysis of vascular-like network formed inside the hydrogels and the composite ($n = 6$). Cell morphology was visualized by staining for actin with Alexa Fluor 568 Phalloidin shown in red. Cell nuclei were stained with 4′,6-diamidino-2-phenylindole (DAPI) shown in blue. Nanofibers were labeled with F8BT shown in green. Scale bars, 100 μm. Statistical significance was calculated by one-way ANOVA with the Dunnett's post hoc test. Comparison was performed between groups. ##$P < 0.01$, ####$P < 0.0001$. Data are presented as means ± SEM.

$CD86^+$ macrophages were identified in the 150-Pa composite than in the 80-Pa hydrogel [150-Pa composite: 70.0% versus 80-Pa hydrogel: 61.2% ($P < 0.01$); Fig. 4, C and D]. Among these $CD86^+$ cells, there were a larger number of $CD206^+CD86^+$ cells inside the composite (22.2% versus 13.9%, $P < 0.01$), leading to a greater shift in macrophage phenotype toward the M2 subtype inside the composite as compared with the 80-Pa hydrogel [$CD206^+/CD86^+$: 0.318 versus 0.227 ($P < 0.05$); Fig. 4E]. In addition, the double identity of macrophages ($CD86^+CD206^+$) suggests that the porous and more compliant hydrogel/composite matrix may be slowing down or reversing M1 polarization of some macrophages induced by inflammatory response from the placement of foreign materials, other than directly inducing M2 polarization of the macrophages.

We also investigated composite-mediated macrophage polarization in vitro. Mouse bone marrow–derived macrophages cultured within the 150-Pa composite for 4 days, when compared to those within the 150-Pa hydrogel, had lower expression of M1-related genes [CD86: 2.5 versus 5.8 ($P < 0.05$) and CCR7: 3.0 versus 15.4 ($P < 0.0001$); figs. S17A and S18]. When macrophages were exposed to lipopolysaccharide and interferon-γ, both of which have been shown to polarize macrophages toward M1 phenotypes (*24*), the composite, compared to the 150-Pa hydrogel, attenuated expression of M1-related genes, including tumor necrosis factor–α (TNFα) and interleukin-6 (IL-6) [TNFα: 2.5 versus 11.3 ($P < 0.0001$) and IL-6: 1.8 versus 11.4 ($P < 0.0001$); fig. S17B]. In contrast, when macrophages were induced by IL-4, a well-established stimulus for M2 macrophages (*25*), the composite, compared to the 150-Pa hydrogel, increased the expression of M2-related genes, such as Arg1 and CD206 [Arg1: 4.2 versus 1.5 ($P < 0.001$) and CD206: 5.0 versus 2.4 ($P < 0.001$); fig. S17C].

Composite-mediated high expression of angiogenesis-related genes

We studied whether our composite-mediated angiogenic gene expression using an angiogenesis polymerase chain reaction (PCR) array. A series of angiogenesis-related genes had been substantially up-regulated by the 150-Pa composite compared to the phosphate-buffered saline (PBS) control (Fig. 5, A and B, and fig. S19). For example, expression of chemokine ligand 2 (CCL2), which plays a role in recruiting monocytes/macrophages to the graft site (*26*), was found to be 14.6-, 53.0-, and 10.5-fold higher in the composite compared to that detected in the PBS control group at PODs 3, 7, and 14, respectively. Other cytokines, such as CXCL2 and IL-1β, both showed high expression at PODs 3 and 7 but returned to baseline at POD 14. Several specific angiogenic factors, such as vascular endothelial growth factor D (VEGF-D) (*27*), displayed 7.2- and 5.0-fold higher expression at PODs 7 and 14, respectively. In addition, expression of cell adhesion molecules, such as fibronectin 1 (FN1), was significantly higher in the composite compared with PBS control [POD 3: 3.2-fold ($P < 0.05$), POD 7: 12.7-fold ($P < 0.0001$), and POD 14: 2.2-fold ($P < 0.05$)]. Matrix metallopeptidase 9 (MMP9) (*28*), which is involved in degrading ECM and vascular remodeling, was up-regulated at all time points [POD 3: 8.0-fold ($P < 0.05$), POD 7: 121.4-fold, and POD 14: 32.7-fold ($P < 0.0001$)]. Other types of proteases, including MMP2 (5.7-fold, $P < 0.01$) and MMP3 (13.5-fold, $P < 0.001$), showed significantly higher expression only at POD 14. Some peptidase inhibitors, including tissue inhibitors of metalloproteinases (TIMPs) 1 and 2, were also highly expressed at PODs 7 and 14 [TIMP1: POD 7, 32.7-fold ($P < 0.001$) and POD 14, 4.8-fold ($P < 0.01$); TIMP2: POD 7, 2.6-fold ($P < 0.05$) and POD 14, 3.7-fold ($P < 0.01$)].

We next compared the expression of angiogenic genes between the 150-Pa composite and the 150-Pa hydrogel (Fig. 5C and fig. S20). In particular, Anpep (8.0 versus 0.9, $P < 0.001$), VEGF-D (7.2 versus 0.4, $P < 0.05$), and FN1 (12.7 versus 2.1, $P < 0.01$) were expressed significantly higher in the composite. Several receptors, including VEGFR1 [Flt1: 2.0 versus 0.4 ($P < 0.01$)], Itga5 (2.6 versus 0.8, $P < 0.001$), and Itgb3 (2.9 versus 0.7, $P < 0.05$), were also highly expressed

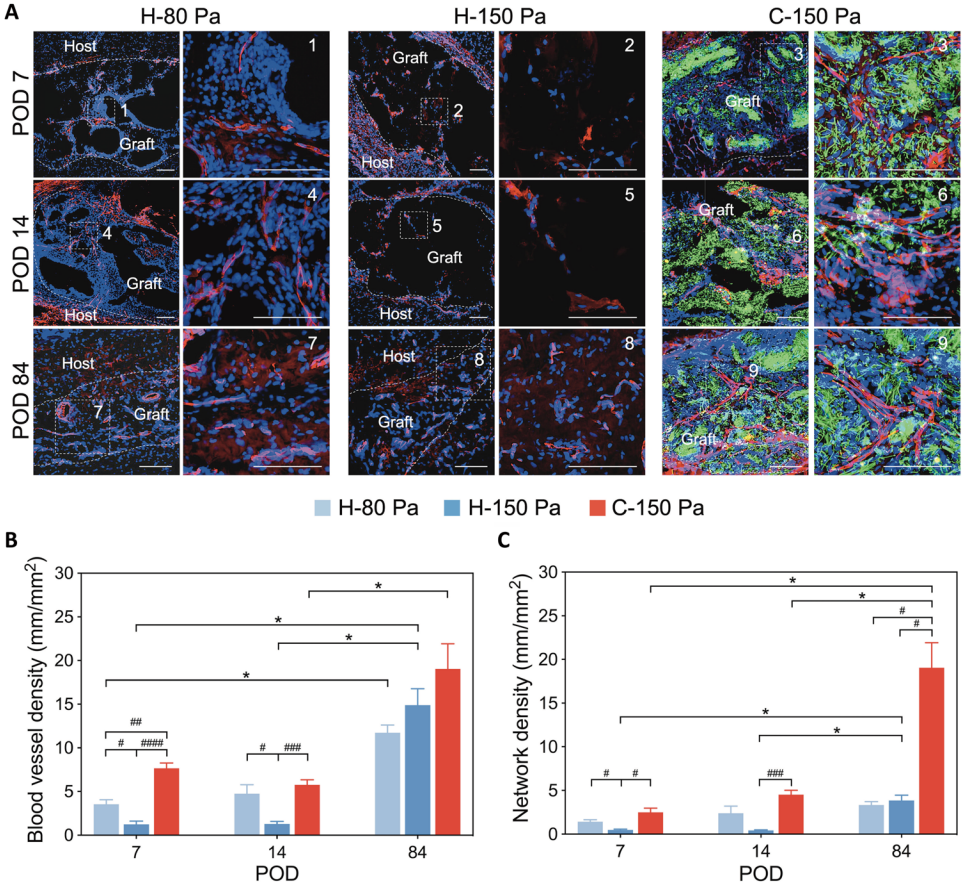

Fig. 3. Improved angiogenesis inside composite after subcutaneous implantation. (**A**) Host vascular cell infiltration in the injected 80- and 150-Pa HA hydrogels and the 150-Pa composite at PODs 7, 14, and 84. Nanofibers were labeled with F8BT shown in green. Cells were stained with RECA-1 for endothelial cells (shown in red) and with DAPI for nuclei (shown in blue). Scale bars, 100 μm. (**B** and **C**) Quantitative analysis of the densities of the blood vessels (B) and the blood vessel network (C) inside the hydrogels and the composite ($n = 6$). Statistical significance was calculated by two-way ANOVA with the Dunnett's post hoc test. Hash key (#) denotes the comparison between groups. Asterisk indicates the comparison between time points. # or *$P < 0.05$, ##$P < 0.01$, ###$P < 0.001$, ####$P < 0.0001$. Data are presented as means ± SEM.

in the composite. Peptidase inhibitors, including TIMP1 (32.7 versus 2.5, $P < 0.05$) and TIMP2 (2.6 versus 0.7, $P < 0.01$), exhibited increased expression in the composite. Collectively, these results clarify that our composite mediates high expression of pro-angiogenic genes, which facilitate the ingrowth of host blood vessels, vascular maturation, and remodeling inside the composite.

Composite-mediated angiogenesis in a rabbit soft tissue defect repair model

We further investigated our composite-mediated host cellular infiltration in a rabbit model for soft tissue defect repair. We developed a protocol to create standardized circular defects within the inguinal fat pads of rabbit using a circular punch (volume, 1 ml). We then injected either composite (1 ml; G′ = 150 Pa or G_0' = 80 Pa) or one of the two hydrogel controls (1 ml; G′ = 80 and 150 Pa) to adequately fill the defect (Fig. 6A). The defects filled with hydrogels appeared transparent, whereas those with composite appeared whitish, similar to native fat (fig. S21). At POD 14, host blood vessels ($CD31^+$) grew into the 80-Pa hydrogel and the 150-Pa composite but not the 150-Pa hydrogel. A boundary between the 150-Pa hydrogel and the surrounding host tissue was evident. Macrophages ($CD68^+$ and $CD206^+$) also infiltrated the 80-Pa hydrogel and the 150-Pa composite but not the 150-Pa hydrogel (Fig. 6B). By POD 42, the 150-Pa composite and the 150-Pa hydrogel yielded similar shape retention, both being greater than that of the 80-Pa hydrogel (fig. S21). Blood vessels could be identified at the periphery of the defect site filled with 150-Pa hydrogel and the boundary with the host tissue (Fig. 6C), and $CD68^+$ pan macrophages and $CD206^+$ pro-regenerative macrophages were not found around the defect site (Fig. 6D). Blood vessels spread broadly within the 150-Pa composite at POD 42. These host blood vessels infiltrated the composite to a greater degree and in a broader area, presenting a notably higher density of blood vessels inside the sample region than the 150-Pa hydrogel ($P < 0.05$; Fig. 6E). These results confirm the ability of the composite to facilitate the ingrowth of host blood vessels into a large soft tissue defect site.

DISCUSSION

We developed a mechanically tunable nanofiber-hydrogel composite that mimics the structural properties of adipose tissue ECM and promotes host vascularization. The unique feature of this nanofiber-hydrogel composite is the interfacial bonding between nanofiber surfaces and the hydrogel network. This bonding provides an effective approach to improving the stiffness of the composite with relatively low fiber loading while also maintaining critical pore size in the hydrogel phase. Our results show that the composite can promote cellular infiltration, revascularization, and host tissue integration into the scaffold. In addition, this nanofiber-hydrogel composite provides soft tissue restoration in an injectable form without the use of exogenous growth factors, thus enhancing its clinical translatability.

The degradation behavior of the composite is important to cell infiltration and tissue remodeling. Degradation is mediated by the enzymatic hydrolysis and infiltrated cells inside the composite. The HA hydrogel is first degraded by hyaluronidase in vivo, as was shown previously (*29*). The degraded HA fragments can induce angiogenesis (*30*). PCL degrades primarily through bulk hydrolysis mechanism (*31*). Our porous structure of composite allowed the infiltration of host cells, including macrophages and endothelial cells, and led to increased concentrations of secreted factors locally, such as MMPs and VEGF-D, to remodel the matrix and promote angiogenesis inside the composite. In particular, activated macrophages secrete hyaluronidase (*32*) and are likely to accelerate HA degradation as they migrated through the composite, whereas the PCL fibers remained

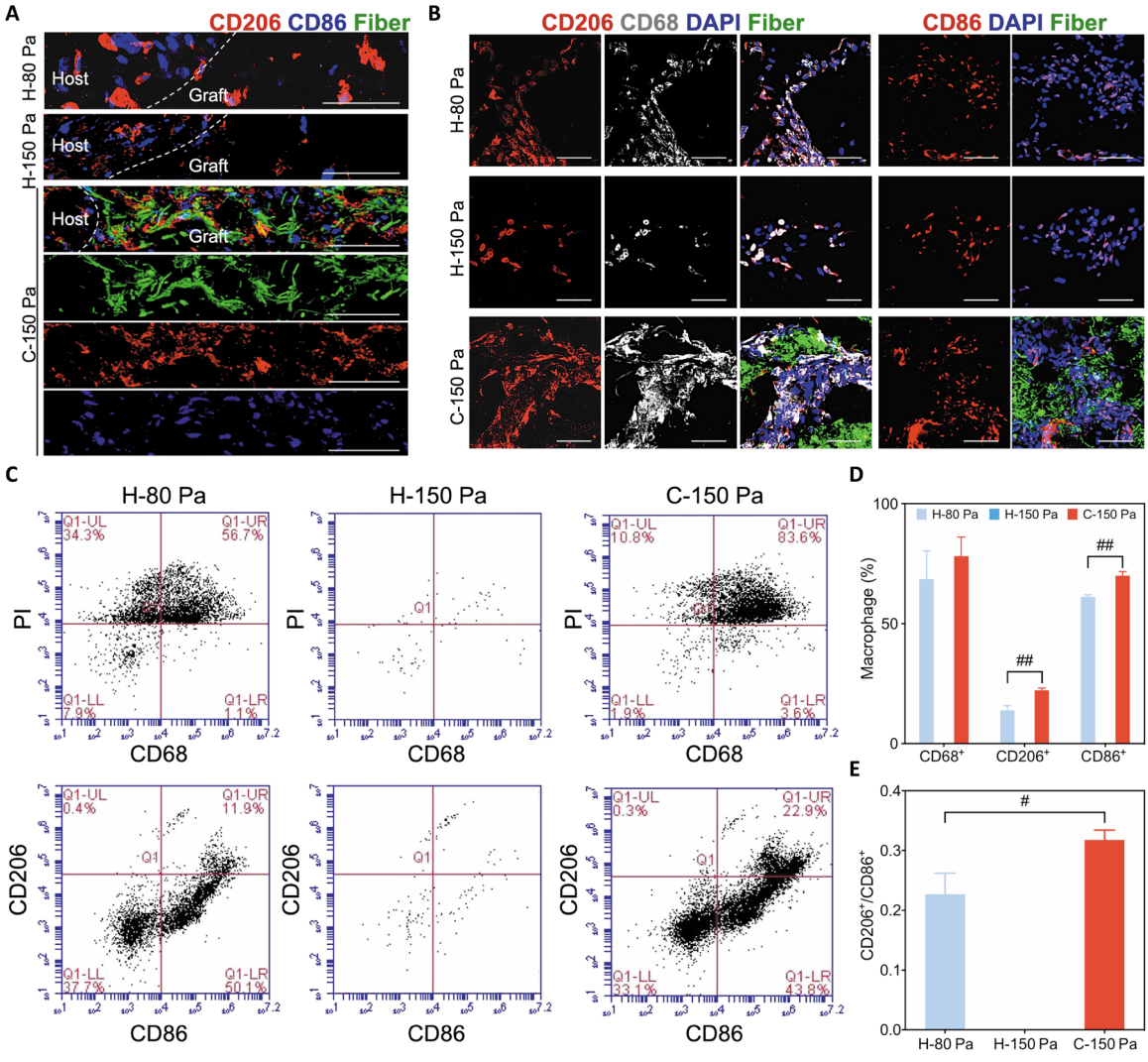

Fig. 4. Infiltration of macrophages into composite and hydrogels and their phenotypes. (**A**) Macrophages infiltrated into 80 and 150-Pa hydrogels and 150-Pa composite at POD 7. Elongated CD206$^+$ macrophages were found inside the composite. Macrophages were stained with CD206 (shown in red) and CD86 (shown in blue). PCL nanofibers were labeled with F8BT shown in green. Scale bars, 100 μm. (**B**) Macrophages observed inside the composite and the hydrogels at POD 14. Macrophages were stained with CD206 (red), CD68 (gray), and CD86 (red). Cell nuclei were stained with DAPI in blue. Scale bars, 100 μm. (**C** to **E**) Quantitative analysis of infiltrated macrophages inside the composite and the hydrogels by flow cytometry ($n = 3$). Statistical significance was calculated by one-way ANOVA with the Dunnett's post hoc test to compare between groups. #$P < 0.05$, ##$P < 0.01$. Data are presented as means ± SEM.

discernable even after 3 months while the cells remodeled around them. PCL fibers could last more than 6 to 18 months in vivo based on our initial observation and data reported in the literature (*33*).

Previous studies have investigated the effect of hydrogel G′ on cellular infiltration in HA hydrogels. However, these HA hydrogel scaffolds exhibit G′ that are 4- to 10-fold greater than scaffolds used in this study (*34*). We observed markedly decreased cell migration in the 150-Pa hydrogel when compared to the softer 80-Pa hydrogel. Vascularization is also minimal throughout the 150-Pa hydrogel, especially when compared to the softer hydrogel of 80 Pa. The 80-Pa hydrogel, however, is not feasible for soft tissue reconstruction, given its limited persistence after in vivo implantation. Simply increasing cross-linking density in the hydrogel to improve its G′ does not resolve this issue because it renders the hydrogel impermeable to cell infiltration and migration. The addition of surface bonding of PCL nanofiber fragments to HA network in the 80-Pa hydrogel resulted in a composite that exhibited enhanced mechanical stiffness with a low fraction [1 to 3% (w/w)] of PCL fibers, as well as improved persistence without hampering cell migration and host tissue infiltration compared to hydrogel controls. For this study, we only included 1% of the PCL nanofiber fragments into the composite to ensure good injectability through a small-diameter needle. The covalent bonding was introduced to confer substantial mechanical reinforcement effect even at such a low weight fraction. The average porosities of hydrogels and composite were calculated on the basis of their compositions. Our 80- and 150-Pa hydrogels had average porosities of 99.6% and 99.2%, respectively. The 1% (w/w) PCL fiber loading in the 150-Pa composite only slightly reduced the porosity of the entire matrix to 98.7%. However, the mesh size or pore size of the composite is difficult to determine because of the biphasic nature of the material. With only 1% fiber loading, we do not believe its effect on pore size distribution in the hydrogel phase will be substantial. The composite achieved the cell infiltration

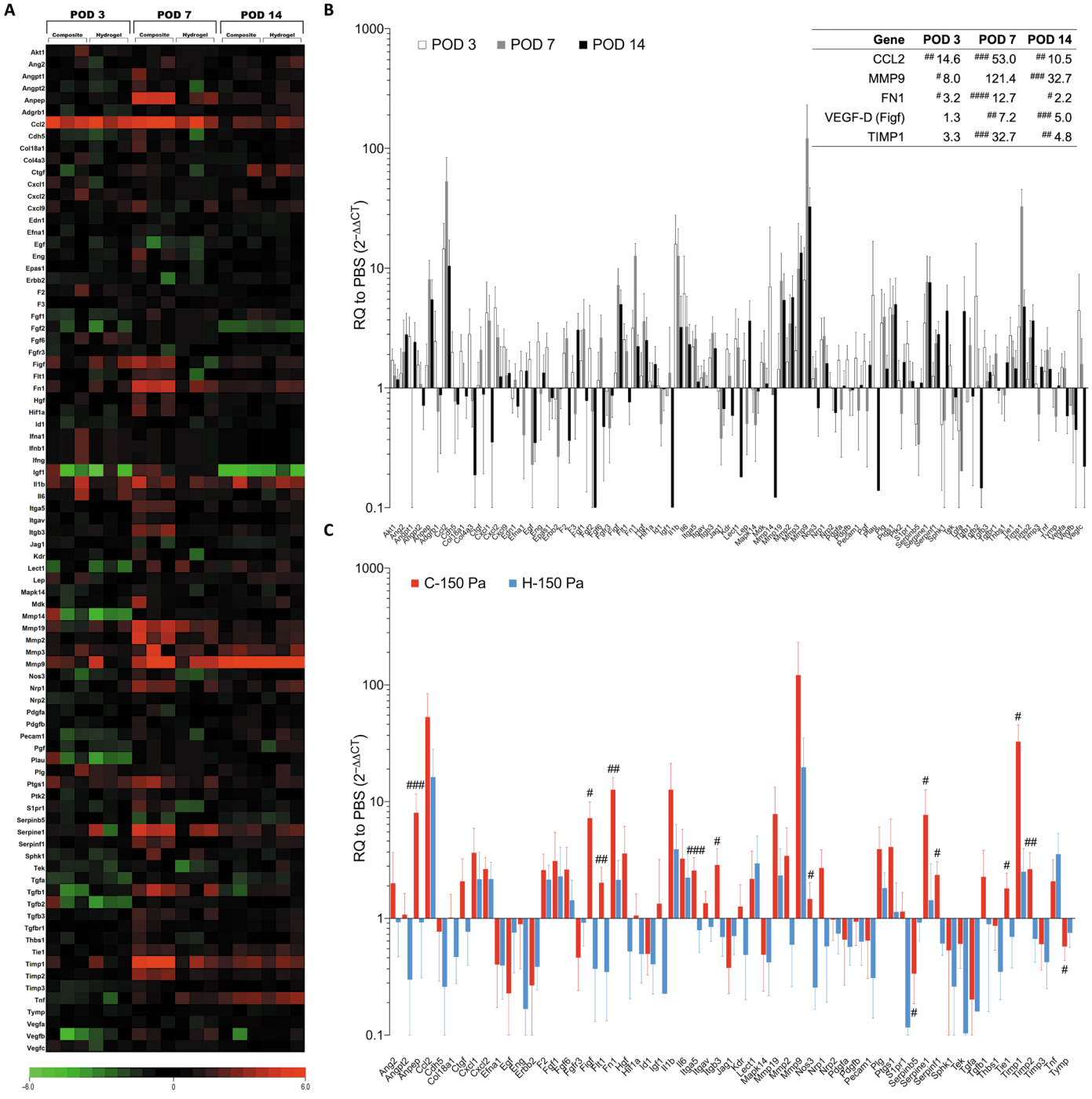

Fig. 5. Composite-mediated high expression of angiogenesis-related genes. (**A**) Heat map analysis of angiogenesis-related gene expression in the 150-Pa composite and the 150-Pa hydrogel at PODs 3, 7, and 14. (**B**) Relative quantification (RQ) for fold change of angiogenesis-related gene expression between the 150-Pa composite and the PBS control. (**C**) Comparison of angiogenesis-related gene expression between the 150-Pa composite and the 150-Pa hydrogel at POD 7 ($n = 3$). Statistical significance was calculated by Student's t test. #$P < 0.05$, ##$P < 0.01$, ###$P < 0.001$, ####$P < 0.0001$. Data are presented as means ± SEM.

and angiogenic property by the porous HA hydrogel ($G_0' = 80$ Pa) and macrophage conditioning, although nanofiber presence also appeared to facilitate cell migration.

We found that a blood vessel network developed and persisted in the 150-Pa composite at 3 months after injection. This angiogenesis response is likely due to the high porosity, low stiffness, and cell-permeable nature of the composite that relates to the role of recruited macrophages (*35*, *36*). One distinct advantage of our composite material lies with its ability to allow infiltration of host monocytes and macrophages into the composite. We observed a large number of macrophages clustered along the fibers within our composite. Among these macrophages, there were a large number of "pro-regenerative"

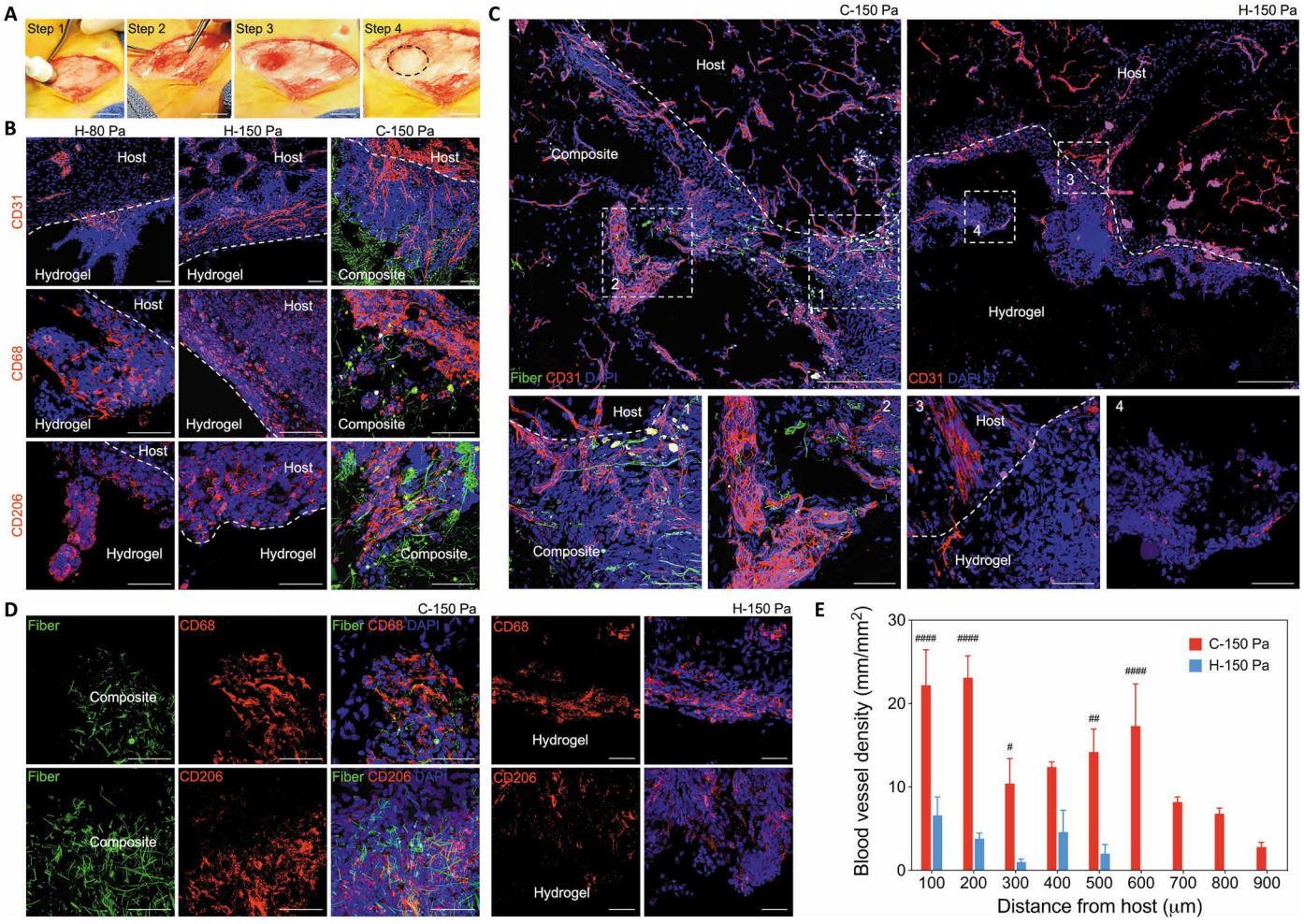

Fig. 6. Composite-mediated angiogenesis at the rabbit fat tissue defect site. (**A**) General procedure for creating defects in the inguinal fat pad in a rabbit model (steps 1 to 3) and injection with the composite (step 4). Scale bars, 10 mm. (**B**) Host blood vessel growth into the 80- and 150-Pa hydrogels and the 150-Pa composite at POD 14. Endothelial cells were stained with CD31 in red. $CD68^+$ was used as a pan macrophage marker; $CD206^+$ labeled pro-regenerative macrophages. Macrophages were stained with CD68 (red) and CD206 (red). Cell nuclei were stained with DAPI in blue. Fibers were F8BT-labeled (green). Scale bars, 100 μm. (**C**) Host blood vessel growth into the 150-Pa hydrogel and the 150-Pa composite at POD 42. Scale bars, 500 μm. (**D**) CD68-marked pan macrophages; CD206-labeled pro-regenerative macrophages. Scale bars, 100 μm. (**E**) Quantitative analysis of the distribution of blood vessels inside the 150-Pa composite and the 150-Pa hydrogel at POD 42 ($n = 4$). Statistical significance was calculated by two-way ANOVA with the Bonferroni's post hoc test. #$P < 0.05$, ##$P < 0.01$, ####$P < 0.0001$. Data are presented as means ± SEM.

$CD206^+$ cells (Fig. 4). This type of pro-regenerative macrophage has previously been shown to increase neovascularization (*22*, *36*). Furthermore, we found that the composite enriched chemokines, such as CCL2 (*37*), which played a role in recruiting monocytes/macrophages and endothelial progenitors into the composite. Macrophages secreted high concentrations of MMP9, enabling degradation of the ECM and recruitment of more inflammatory cells into the composite (*28*). In addition, the degradation products of HA may provide additional pro-angiogenic signal (*30*) and further facilitate blood vessel development in the local milieu. The PCL fibers continue to provide mechanical support to improve the structural integrity, allowing blood vessel development inside the composite. Accumulation of macrophages inside the composite produced other types of MMPs (MMP2, MMP3, and MMP19), VEGF-D, and FN1, all of which facilitated angiogenesis, vascular remodeling, and maturation inside the composite (fig. S22) (*38*). In contrast, the HA hydrogel without PCL fibers but cross-linked to the same stiffness ($G' = 150$ Pa), despite also having degraded HA fragments that could encourage angiogenesis, limits degradation and cell migration to the periphery of the implant. The HA hydrogel of 80-Pa allows host cell infiltration and angiogenesis inside its matrix, but the fast degradation of HA limits the structural integrity of the hydrogel, leading to less blood vessel networks inside the implant. Our results confirm that both porosity and nanofibers are required to realize the substantial cell infiltration, angiogenesis, and tissue regeneration and remodeling.

Note that hydrogels with a larger pore structure have also been explored using other approaches. For example, Griffin *et al.* (*39*) developed a microporous annealed particle hydrogel and achieved cell infiltration with rapid tissue regeneration. Using 30- to 150-μm hydrogel particles, they formed an annealed particle network with interconnected micropores of 10 to 35 μm using Factor XIII (FXIIIa) to cross-link the contact surfaces of the hydrogel particles and thus to stabilize the hydrogel network. This interconnected pore network was shown to have facilitated cell infiltration and angiogenesis. Compared with this approach, our composite design relies on the intrinsic pore size and structure of the porous hydrogel and incorporated nanofibers, without requiring careful

control of pore structure and interconnectivity of microgel particles, which may be difficult to achieve in vivo after injection.

This study highlights the use of the body's own abilities for tissue remodeling and regeneration. Even without the presence of exogenous cytokines or cells loaded into the composite before injection, angiogenesis was observed inside the composite with a longer-lasting shape retention outcome. In contrast, most recent studies have focused on the use of exogenous factors or cellular cues in conjunction with scaffolds. Even with the addition of these factors, the cellular infiltration and vascular ingrowth effects have been modest.

The composite used in this study is intended as in situ forming material. In consideration of clinical application of our composite, patients with typical breast lumpectomy are often left with postoperative breast deformities (*40*). Intraoperative delivery of our composite after breast tumor resection would allow for immediate soft tissue restoration in a single-stage procedure. The in situ gelling nature of our composite allows conformation to the irregular contour defects created after tumor extirpation. The gelation process usually takes several hours to form stable matrix without requiring additives or generating by-products. This feature provides an ample time window for injection after component mixing and affords the ability to shape before the composite is fully set. In the case where soft tissue reconstruction is not performed concurrently, in situ gelling composite allows for a minimally invasive percutaneous delivery, which is well tolerated in the outpatient clinical setting. Our results from the rabbit model also demonstrated a case for repair immediately after tissue removal or defect repair.

Generating larger volumes of soft tissue with the composite alone will be challenging because spontaneous cell infiltration to reconstruct soft tissue is a slow and gradual process. Nonetheless, the composite may be used in conjunction with autologous or allogeneic adipose-derived stem and progenitor cells to augment the effect. The porous and angiogenic nature of the composite argues favorably for its additional function as carrier for these cells after transplantation. In addition, the mechanism of composite-mediated macrophage polarization and tissue ingrowth still needs to be further expanded, including the effect of matrix stiffness on macrophage conditioning (*41*). The fiber-hydrogel composite may create a unique microenvironment that exerts a different mechanobiology to macrophages and endothelial cells. The exact mechanism will require more detailed signaling dynamic study, which is part of an on-going investigation that we will report in the near future.

Beyond the data presented here on the unique structural design, composition, and property of the composite, the excellent safety track record of HA and PCL in clinical devices argues favorably for the future clinical translation of this composite. Translational activities are currently underway to develop an injectable biodegradable filler product for soft tissue augmentation in aesthetic and reconstructive cases, which follow a U.S. Food and Drug Administration regulatory pathway for a class III medical device.

In summary, we have developed a unique nanofiber-hydrogel composite that mimics the microarchitecture and mechanical properties of soft tissue matrix. The high porosity and integrated nanofiber fragments promote host cell infiltration, macrophage conditioning toward pro-regenerative phenotype, and angiogenetic response within the composite, without the addition of any exogenous cells or factors, thus building the foundation for soft tissue restoration in defect repair. Our goal is to translate this approach into a minimally invasive solution for the numerous patients suffering from soft tissue losses.

MATERIALS AND METHODS

Study design

The objective of this study is to develop a nanofiber-hydrogel composite with the interfacial bonding between the fibers and hydrogel matrix for soft tissue reconstruction and regeneration. The composite with the interfacial bonding between fibers and hydrogels could maintain their structure and simultaneously allow cell migration and infiltration inside the matrix. The interfacial bonding between fibers and hydrogels was examined by rheological tests. In vitro cell migration and vascularization studies were designed to investigate cell migration and organization inside the matrix. The ability of the composite for cell infiltration was tested by subcutaneous injection of the composite ($n = 6$). PCR array assay was applied to investigate the mechanism of composite-mediated cell infiltration and angiogenesis in vivo ($n = 3$). The potential of the composite for soft tissue regeneration was also tested in a rabbit soft tissue defect model ($n = 4$). The immunostaining images were evaluated and analyzed by a technician in a blinded manner. There were no data excluded from this study. Individual subject-level data are reported in data file S1. Primary antibodies used in the study are listed in table S1.

Statistical analysis

Data are shown as means ± SEM. Data were analyzed using GraphPad Prism software (GraphPad Software Inc.) by Student's *t* test (unpaired and two-tailed), one- or two-way ANOVA (analysis of variance), followed by Dunnett's or Bonferroni's post hoc test as needed. The values were considered significantly different at $P < 0.05$.

SUPPLEMENTARY MATERIALS

stm.sciencemag.org/cgi/content/full/11/490/eaau6210/DC1

Materials and Methods

Fig. S1. Controlling carboxylic group density on the PCL nanofiber by changing plasma treatment time.

Fig. S2. Controlling the length of nanofiber fragments and the reproducibility of composites.

Fig. S3. The molecular structure of HA hydrogel as a comparison for the composite.

Fig. S4. Characterization of mechanical properties of the composite.

Fig. S5. Fluorescence image showing the distribution of nanofibers inside the composite.

Fig. S6. Fluorescence image showing phase separation of carboxyl-functionalized nanofibers from the hydrogel.

Fig. S7. Vascular-like network formation in HA hydrogels.

Fig. S8. hASCs cocultured with human umbilical vein endothelial cells inside the 80-Pa hydrogel.

Fig. S9. Infiltration of host vascular cells into the 150-Pa composite at POD 7.

Fig. S10. Blood vessels inside the 150-Pa composite at POD 14.

Fig. S11. Well-formed blood vessel networks inside the 150-Pa composite at POD 84.

Fig. S12. Vascular maturation inside the 150-Pa composite at PODs 7, 14, and 84.

Fig. S13. Vascular network inside the 150-Pa composite at POD 84 shown in the 3D image.

Fig. S14. Macroscopic images of subcutaneously injected 80- and 150-Pa hydrogels and 150-Pa composite at PODs 7 and 14.

Fig. S15. Perfusable blood vessels observed in the 150-Pa composite examined by indocyanine green angiography.

Fig. S16. Macrophages infiltrated 80- and 150-Pa hydrogels and 150-Pa composite at POD 14.

Fig. S17. Composite-mediated macrophage polarization in vitro.

Fig. S18. Macrophage morphologies inside the 80- and 150-Pa hydrogels and 150-Pa composite under normal conditions.

Fig. S19. Angiogenesis-related gene expression inside the 150-Pa composite.

Fig. S20. Comparison of angiogenic gene expression between the composite and the hydrogel with the same G′ of 150 Pa.

Fig. S21. Composite-mediated tissue regeneration in a rabbit soft tissue defect model.

Fig. S22. Processes involved in composite-mediated angiogenesis.

Table S1. Primary antibodies used in this study.

Data file S1. Individual subject-level data for quantitative analysis.

References (*42*–*48*)

REFERENCES AND NOTES

1. K. M. Patel, L. M. Hill, M. E. Gatti, M. Y. Nahabedian, Management of massive mastectomy skin flap necrosis following autologous breast reconstruction. *Ann. Plast. Surg.* **69**, 139–144 (2012).
2. B. Tsoi, N. I. Ziolkowski, A. Thoma, K. Campbell, D. O'Reilly, R. Goeree, Safety of tissue expander/implant versus autologous abdominal tissue breast reconstruction in postmastectomy breast cancer patients: A systematic review and meta-analysis. *Plast. Reconstr. Surg.* **133**, 234–249 (2014).
3. R. D. Largo, L. A. H. Tchang, V. Mele, A. Scherberich, Y. Harder, R. Wettstein, D. J. Schaefer, Efficacy, safety and complications of autologous fat grafting to healthy breast tissue: A systematic review. *J. Plast. Reconstr. Aesthet. Surg.* **67**, 437–448 (2014).
4. N. H. Attenello, C. S. Maas, Injectable fillers: Review of material and properties. *Facial Plast. Surg.* **31**, 29–34 (2015).
5. P. Lucey, D. J. Goldberg, Complications of collagen fillers. *Facial Plast. Surg.* **30**, 615–622 (2014).
6. E. Bellas, T. J. Lo, E. P. Fournier, J. E. Brown, R. D. Abbott, E. S. Gil, K. G. Marra, J. P. Rubin, G. G. Leisk, D. L. Kaplan, Injectable silk foams for soft tissue regeneration. *Adv. Healthc. Mater.* **4**, 452–459 (2015).
7. D. A. Young, D. O. Ibrahim, D. Hu, K. L. Christman, Injectable hydrogel scaffold from decellularized human lipoaspirate. *Acta Biomater.* **7**, 1040–1049 (2011).
8. D. M. Varma, G. T. Gold, P. J. Taub, S. B. Nicoll, Injectable carboxymethylcellulose hydrogels for soft tissue filler applications. *Acta Biomater.* **10**, 4996–5004 (2014).
9. D. Atashroo, J. Raphel, M. Chung, K. Paik, A. Parisi-Amon, A. McArdle, K. Senarath-Yapa, E. Zielins, R. Tevlin, C. Duldulao, G. G. Walmsley, M. Hu, A. Momeni, B. Domecus, J. Rimsa, L. Greenberg, G. C. Gurtner, M. T. Longaker, D. C. Wan, Studies in fat grafting: Part II. Effects of injection mechanics on material properties of fat. *Plast. Reconstr. Surg.* **134**, 39–46 (2014).
10. S. Khetan, M. Guvendiren, W. R. Legant, D. M. Cohen, C. S. Chen, J. A. Burdick, Degradation-mediated cellular traction directs stem cell fate in covalently crosslinked three-dimensional hydrogels. *Nat. Mater.* **12**, 458–465 (2013).
11. E. M. Sussman, M. C. Halpin, J. Muster, R. T. Moon, B. D. Ratner, Porous implants modulate healing and induce shifts in local macrophage polarization in the foreign body reaction. *Ann. Biomed. Eng.* **42**, 1508–1516 (2014).
12. B. N. Brown, R. Londono, S. Tottey, L. Zhang, K. A. Kukla, M. T. Wolf, K. A. Daly, J. E. Reing, S. F. Badylak, Macrophage phenotype as a predictor of constructive remodeling following the implantation of biologically derived surgical mesh materials. *Acta Biomater.* **8**, 978–987 (2012).
13. Y. Zhu, S. Hideyoshi, H. Jiang, Y. Matsumura, J. L. Dziki, S. T. LoPresti, L. Huleihel, G. N. F. Faria, L. C. Fuhrman, R. Lodono, S. F. Badylak, W. R. Wagner, Injectable, porous, biohybrid hydrogels incorporating decellularized tissue components for soft tissue applications. *Acta Biomater.* **73**, 112–126 (2018).
14. J. L. Holloway, A. M. Lowman, M. R. VanLandingham, G. R. Palmese, Interfacial optimization of fiber-reinforced hydrogel composites for soft fibrous tissue applications. *Acta Biomater.* **10**, 3581–3589 (2014).
15. J. Coburn, M. Gibson, P. A. Bandalini, C. Laird, H.-Q. Mao, L. Moroni, D. Seliktar, J. Elisseeff, Biomimetics of the extracellular matrix: An integrated three-dimensional fiber-hydrogel composite for cartilage tissue engineering. *Smart Struct. Syst.* **7**, 213–222 (2011).
16. Y. M. Shin, T. G. Kim, J.-S. Park, H.-J. Gwon, S. I. Jeong, H. Shin, K.-S. Kim, D. Kim, M.-H. Yoon, Y.-M. Lim, Engineered ECM-like microenvironment with fibrous particles for guiding 3D-encapsulated hMSC behaviours. *J. Mater. Chem. B* **3**, 2732–2741 (2015).
17. X. Z. Shu, Y. Liu, F. S. Palumbo, Y. Luo, G. D. Prestwich, In situ crosslinkable hyaluronan hydrogels for tissue engineering. *Biomaterials* **25**, 1339–1348 (2004).
18. X. Jiang, G. T. Christopherson, H.-Q. Mao, The effect of nanofibre surface amine density and conjugate structure on the adhesion and proliferation of human haematopoietic progenitor cells. *Interface Focus* **1**, 725–733 (2011).
19. X. Li, X. Liu, B. Josey, C. J. Chou, Y. Tan, N. Zhang, X. Wen, Short laminin peptide for improved neural stem cell growth. *Stem Cells Transl. Med.* **3**, 662–670 (2014).
20. X. Li, X. Liu, N. Zhang, X. Wen, Engineering in situ cross-linkable and neurocompatible hydrogels. *J. Neurotrauma* **31**, 1431–1438 (2014).
21. D. L. Hutton, R. Kondragunta, E. M. Moore, B. P. Hung, X. Jia, W. L. Grayson, Tumor necrosis factor improves vascularization in osteogenic grafts engineered with human adipose-derived stem/stromal cells. *PLOS ONE* **9**, e107199 (2014).
22. L. R. Madden, D. J. Mortisen, E. M. Sussman, S. K. Dupras, J. A. Fugate, J. L. Cuy, K. D. Hauch, M. A. Laflamme, C. E. Murry, B. D. Ratner, Proangiogenic scaffolds as functional templates for cardiac tissue engineering. *Proc. Natl. Acad. Sci. U.S.A.* **107**, 15211–15216 (2010).
23. F. Y. McWhorter, T. Wang, P. Nguyen, T. Chung, W. F. Liu, Modulation of macrophage phenotype by cell shape. *Proc. Natl. Acad. Sci. U.S.A.* **110**, 17253–17258 (2013).
24. G. J. Nau, J. F. L. Richmond, A. Schlesinger, E. G. Jennings, E. S. Lander, R. A. Young, Human macrophage activation programs induced by bacterial pathogens. *Proc. Natl. Acad. Sci. U.S.A.* **99**, 1503–1508 (2002).
25. G. Casella, L. Garzetti, A. T. Gatta, A. Finardi, C. Maiorino, F. Ruffini, G. Martino, L. Muzio, R. Furlan, IL4 induces IL6-producing M2 macrophages associated to inhibition of neuroinflammation in vitro and in vivo. *J. Neuroinflammation* **13**, 139 (2016).
26. S. L. Deshmane, S. Kremlev, S. Amini, B. E. Sawaya, Monocyte chemoattractant protein-1 (MCP-1): An overview. *J. Interferon Cytokine Res.* **29**, 313–326 (2009).
27. L. Marconcini, S. Marchiò, L. Morbidelli, E. Cartocci, A. Albini, M. Ziche, F. Bussolino, S. Oliviero, c-*fos*-induced growth factor/vascular endothelial growth factor D induces angiogenesis in vivo and in vitro. *Proc. Natl. Acad. Sci. U.S.A.* **96**, 9671–9676 (1999).
28. E. Zajac, B. Schweighofer, T. A. Kupriyanova, A. Juncker-Jensen, P. Minder, J. P. Quigley, E. I. Deryugina, Angiogenic capacity of M1- and M2-polarized macrophages is determined by the levels of TIMP-1 complexed with their secreted proMMP-9. *Blood* **122**, 4054–4067 (2013).
29. X. Z. Shu, S. Ahmad, Y. Liu, G. D. Prestwich, Synthesis and evaluation of injectable, in situ crosslinkable synthetic extracellular matrices for tissue engineering. *J. Biomed. Mater. Res. A* **79A**, 902–912 (2006).
30. M. Slevin, S. Kumar, J. Gaffney, Angiogenic oligosaccharides of hyaluronan induce multiple signaling pathways affecting vascular endothelial cell mitogenic and wound healing responses. *J. Biol. Chem.* **277**, 41046–41059 (2002).
31. M. A. Woodruff, D. W. Hutmacher, The return of a forgotten polymer—Polycaprolactone in the 21st century. *Prog. Polym. Sci.* **35**, 1217–1256 (2010).
32. E. Puissant, M. Boonen, Monocytes/macrophages upregulate the hyaluronidase HYAL1 and adapt its subcellular trafficking to promote extracellular residency upon differentiation into osteoclasts. *PLOS ONE* **11**, e0165004 (2016).
33. H. Sun, L. Mei, C. Song, X. Cui, P. Wang, The in vivo degradation, absorption and excretion of PCL-based implant. *Biomaterials* **27**, 1735–1740 (2006).
34. R. M. Schweller, Z. J. Wu, B. Klitzman, J. L. West, Stiffness of protease sensitive and cell adhesive PEG hydrogels promotes neovascularization in vivo. *Ann. Biomed. Eng.* **45**, 1387–1398 (2017).
35. K. L. Spiller, R. R. Anfang, K. J. Spiller, J. Ng, K. R. Nakazawa, J. W. Daulton, G. Vunjak-Novakovic, The role of macrophage phenotype in vascularization of tissue engineering scaffolds. *Biomaterials* **35**, 4477–4488 (2014).
36. N. Jetten, S. Verbruggen, M. J. Gijbels, M. J. Post, M. P. J. De Winther, M. M. P. C. Donners, Anti-inflammatory M2, but not pro-inflammatory M1 macrophages promote angiogenesis in vivo. *Angiogenesis* **17**, 109–118 (2014).
37. C. Shi, E. G. Pamer, Monocyte recruitment during infection and inflammation. *Nat. Rev. Immunol.* **11**, 762–774 (2011).
38. T. Ehashi, T. Takemura, N. Hanagata, T. Minowa, H. Kobayashi, K. Ishihara, T. Yamaoka, Comprehensive genetic analysis of early host body reactions to the bioactive and bio-inert porous scaffolds. *PLOS ONE* **9**, e85132 (2014).
39. D. R. Griffin, W. M. Weaver, P. Scumpia, D. Di Carlo, T. Segura, Accelerated wound healing by injectable microporous gel scaffolds assembled from annealed building blocks. *Nat. Mater.* **14**, 737–744 (2015).
40. J. F. Honart, A. S. Reguesse, S. Struk, B. Sarfati, F. Rimareix, H. Alkhashnam, F. Kolb, K. Rem, N. Leymarie, Indications and controversies in partial mastectomy defect reconstruction. *Clin. Plast. Surg.* **45**, 33–45 (2018).
41. T. Okamoto, Y. Takagi, E. Kawamoto, E. J. Park, H. Usuda, K. Wada, M. Shimaoka, Reduced substrate stiffness promotes M2-like macrophage activation and enhances peroxisome proliferator-activated receptor γ expression. *Exp. Cell Res.* **367**, 264–273 (2018).
42. S. H. Lim, X. Y. Liu, H. Song, K. J. Yarema, H.-Q. Mao, The effect of nanofiber-guided cell alignment on the preferential differentiation of neural stem cells. *Biomaterials* **31**, 9031–9039 (2010).
43. C. Yin, L. Ying, P.-C. Zhang, R.-X. Zhuo, E.-T. Kang, K. W. Leong, H.-Q. Mao, High density of immobilized galactose ligand enhances hepatocyte attachment and function. *J. Biomed. Mater. Res.* **67**, 1093–1104 (2003).
44. E. A. Phelps, N. O. Enemchukwu, V. F. Fiore, J. C. Sy, N. Murthy, T. A. Sulchek, T. H. Barker, A. J. Garcia, Maleimide cross-linked bioactive PEG hydrogel exhibits improved reaction kinetics and cross-linking for cell encapsulation and in situ delivery. *Adv. Mater.* **24**, 64–70 (2012).
45. D. P. Nair, M. Podgórski, S. Chatani, T. Gong, W. Xi, C. R. Fenoli, C. N. Bowman, The thiol-Michael addition click reaction: A powerful and widely used tool in materials chemistry. *Chem. Mater.* **26**, 724–744 (2014).
46. X. Li, X. Liu, W. Zhao, X. Wen, N. Zhang, Manipulating neural-stem-cell mobilization and migration in vitro. *Acta Biomater.* **8**, 2087–2095 (2012).
47. D. L. Hutton, W. L. Grayson, Hypoxia inhibits de novo vascular assembly of adipose-derived stromal/stem cell populations, but promotes growth of preformed vessels. *Tissue Eng. Part A* **22**, 161–169 (2016).
48. J. Weischenfeldt, B. Porse, Bone marrow-derived macrophages (BMM): Isolation and applications. *Cold Spring Harb. Protoc.* **2008**, pdb.prot5080 (2008).

Acknowledgments: We thank D. Ding for technical assistance. **Funding:** This work was supported by the U.S. National Institute of Neurological Disorders and Stroke (R21NS085714 to H.-Q.M.), Maryland Stem Cell Research Fund (2018-MSCRFCO-4088 to S.R. and H.-Q.M.), the

National Science Foundation (DMR1410240 to H.-Q.M.), Coulter Foundation Translational Grant (H.-Q.M. and J.M.S.), Cohen Translational Engineering Fund (H.-Q.M. and S.R.), Louis B. Thalheimer Award for Translational Research (H.-Q.M., J.M.S., and S.R.), Abell Foundation Translational Award (H.-Q.M., J.M.S., and S.R.), and Maryland Innovation Initiative (J.M.S.). X.L. acknowledges a postdoctoral fellowship from the Maryland Stem Cell Research Fund (2013MSCRF-00042169) and an AHA Career Development award (18CDA34110314).
Author contributions: X.L. and B.C. contributed to the design, execution, and analysis of all experiments. M.S., C.Z., M.C., Z.Z., G.W., and K.C. contributed to the animal studies, tissue processing, and staining experiments. J.M.-M. and W.G. contributed to the in vitro cell migration and angiogenesis experiments. H.L. contributed to the macrophage polarization experiment and PCR analysis. R.M., X.J., L.C., J.S.C., and J.Y. contributed to the study design and data analysis. H.-Q.M., J.M.S., and S.R. conceived the project and contributed to the study design and result analysis. X.L. and H.-Q.M. prepared the manuscript with inputs from all authors. **Competing interests:** H.-Q.M., J.M.S., S.R., X.L., R.M., J.S.C., and X.J. are coinventors of a U.S. Patent Application US20180050130A1 on "Composite Material for Tissue Restoration." H.-Q.M., J.M.S., S.R., and R.M. are cofounders of LifeSprout Inc., a startup company that has licensed the technology described here. H.-Q.M., J.M.S., S.R., R.M., and K.C. have equity interests in LifeSprout Inc. S.R. and H.-Q.M. receive consulting fees from LifeSprout Inc. J.M.S. is a consultant and speaker for Allergan. Other authors declare that they have no competing financial interests. **Data and materials availability:** All data associated with this study are present in the paper or Supplementary Materials.

Submitted 29 June 2018
Accepted 15 March 2019
Published 1 May 2019
10.1126/scitranslmed.aau6210

Citation: X. Li, B. Cho, R. Martin, M. Seu, C. Zhang, Z. Zhou, J. S. Choi, X. Jiang, L. Chen, G. Walia, J. Yan, M. Callanan, H. Liu, K. Colbert, J. Morrissette-McAlmon, W. Grayson, S. Reddy, J. M. Sacks, H.-Q. Mao, Nanofiber-hydrogel composite–mediated angiogenesis for soft tissue reconstruction. *Sci. Transl. Med.* **11**, eaau6210 (2019).

Science Translational Medicine

Nanofiber-hydrogel composite–mediated angiogenesis for soft tissue reconstruction

Xiaowei Li, Brian Cho, Russell Martin, Michelle Seu, Chi Zhang, Zhengbing Zhou, Ji Suk Choi, Xuesong Jiang, Long Chen, Gurjot Walia, Jerry Yan, Megan Callanan, Huanhuan Liu, Kevin Colbert, Justin Morrissette-McAlmon, Warren Grayson, Sashank Reddy, Justin M. Sacks and Hai-Quan Mao

Sci Transl Med **11**, eaau6210.
DOI: 10.1126/scitranslmed.aau6210

Crafting a (re)constructive composite

To be useful for soft tissue reconstruction, a biomaterial should be compatible with surgical manipulation while providing material properties similar to the native tissue and should not promote scarring or adverse cell activation. Toward this goal, Li *et al*, developed an injectable, biodegradable composite biomaterial composed of hyaluronic acid hydrogel with embedded synthetic polymer fibers. Human cells formed vascular-like networks within the material in vitro, and subcutaneously implanted material showed macrophage infiltration and angiogenesis in rats. Macrophages were polarized toward a pro-regenerative phenotype, and the material facilitated adipose soft tissue defect repair in a rabbit model.

Science Translational Medicine (ISSN 1946-6242) is published by the American Association for the Advancement of Science, 1200 New York Avenue NW, Washington, DC 20005.